Published in final edited form as:
*Sci Transl Med*. 2009 November 4; 1(5): 5ra13. doi:10.1126/scitranslmed.3000111.

# Serum Amyloid P Inhibits Fibrosis Through FcγR-Dependent Monocyte-Macrophage Regulation in Vivo

**Ana P. Castaño**[1,2,*], **Shuei-Liong Lin**[1,2,*], **Teresa Surowy**[3], **Brian T. Nowlin**[1], **Swathi A. Turlapati**[1], **Tejas Patel**[2], **Ajay Singh**[2], **Shawn Li**[3], **Mark L. Lupher Jr.**[3], and **Jeremy S. Duffield**[1,2,†]

[1]Laboratory of Inflammation Research, Harvard Institutes of Medicine, 5th Floor, 4 Blackfan Circle, Boston, MA 02115, USA.

[2]Renal Division, Department of Medicine, Brigham and Women's Hospital and Harvard Medical School, Boston, MA 02115, USA.

[3]Promedior Inc., Malvern, PA 19355, USA.

## Abstract

New therapies that target chronic inflammation with fibrosis are urgently required. Increasing evidence points to innate activation of inflammatory cells in driving chronic organ fibrosis. Serum amyloid P is a naturally circulating soluble pattern recognition receptor, a member of the family of pentraxin proteins. It links danger-associated molecular pattern recognition to Fcγ receptor–mediated phagocytosis. Here we show that fibrosis progression in the mouse kidney is significantly inhibited by therapeutic administration of human serum amyloid P, regulated by activating Fcγ receptors, and dependent on inflammatory monocytes and macrophages, but not fibrocytes. Human serum amyloid P–mediated inhibition of mouse kidney fibrosis correlated with specific binding of human serum amyloid P to cell debris and with subsequent suppression of inflammatory monocytes and kidney macrophages in vitro and in vivo, and was dependent on regulated binding to activating Fcγ receptors and interleukin-10 expression. These studies uncover previously unidentified roles for Fcγ receptors in sterile inflammation and highlight serum amyloid P as a potential antifibrotic therapy through local generation of interleukin-10.

## INTRODUCTION

Many modern human diseases, including those of heart, lung, liver, gut, kidney, brain, and large blood vessels, are characterized by chronic inflammation with fibrosis, loss of microvasculature, loss of organ parenchyma, and loss of function. Increasing evidence points to activation of the innate immune system, recruited in response to tissue injury in these disease processes (1). Currently, few effective therapies target these fibrotic inflammatory diseases. Fibrosis itself causes parenchymal cell ischemia, distortion, and contraction of normal organ architecture and contributes directly to functional demise (2). Despite the prevalence of organ

†To whom correspondence should be addressed. jduffield@rics.bwh.harvard.edu.
*These authors contributed equally to this work.

Author contributions: J.S.D. and M.L.L. designed and performed experiments, interpreted and presented data, and wrote the manuscript. A.P.C, S.L.L., T.S, B.T.N, S.A.T., and S.L performed experiments and interpreted data. T.V.P. and A.S. maintained and analyzed patient cohort.

Competing interests: T.S.,M.L.L., S.L., and J.S.D. own stock options in Promedior, Inc., a company that develops therapeutic agents for the treatment of fibrotic disorders and diseases. M.L.L. is an officer at Promedior, and J.S.D. is a paid member of the Scientific Advisory Board. Promedior has assignment of or license to several patent applications relating to the use of hSAP for treatment of various fibrotic disorders, including kidney fibrosis.

fibrosis, no therapies directly target the fibrotic process. There is a pandemic of such fibrotic diseases of the kidney in Western societies, ultimately leading to organ failure and the need for lifesaving dialysis or organ transplantation.

Both chronic and acute tissue injuries stimulate a primary innate injury response that is broadly similar across all tissues, including the kidney. This response involves the sequential, regulated recruitment and activation of multiple cell populations of hematopoietic and mesenchymal origin (3). The process proceeds through several phases including an initial classical inflammatory influx of neutrophils and monocytes, generation of excessive apoptotic and/or necrotic tissue, recruitment and activation of myofibroblasts, significant extracellular matrix deposition, and dynamic extracellular matrix remodeling. Whether the outcome of this innate injury response is resolution of injury and restoration of normal tissue homeostasis (wound healing) or progressive fibrotic disease is controlled by the type of cell populations that are recruited to and activated at the site of injury. There is accumulating evidence that monocyte-derived cell populations can dynamically control this process through both direct effects on matrix remodeling and indirect effects on regulation of activated myofibroblasts and their precursor populations (4–12).

Serum amyloid P (SAP), also known as pentraxin-2, is a highly conserved, naturally circulating serum protein and one of two short pentraxin protein family members, the other being C-reactive protein (CRP) (13–17). SAP is produced in the liver and circulates as a highly stable 135-kD pentamer (18) composed of five noncovalently linked 27-kD protomers associated into a ring-like structure (19). Each protomer of SAP contains two unique binding sites: a $Ca^{2+}$-dependent ligand-binding site on one face of the protomer and a receptor-binding site on the opposite face for recognition of specific Fcγ receptors (FcγRs) (20). The calcium-dependent ligands recognized by SAP include both pathogen-associated molecular patterns [PAMPs; for example, lipopolysaccharide (LPS) and zymosan] and danger- or damage-associated molecular patterns (DAMPs; for example, DNA, chromatin, and phosphorylethanolamine) presented on the membranes of apoptotic cells. SAP binding to $Ca^{2+}$- dependent ligands promotes subsequent FcγR-dependent phagocytosis (21–26).

Although SAP was initially identified as a minor component of amyloid plaque, which led to its nomenclature (27), it is structurally unrelated to β-amyloid (Aβ) or amyloid precursor protein (28). SAP association with amyloid plaque likely reflects a humoral response to amyloid deposition, because amyloid fibrils are also recognized by SAP as $Ca^{2+}$-dependent ligands. These unique binding activities of SAP and in vitro biology studies suggest that SAP may localize specifically to sites of injury and aid in the removal of damaged tissue and pathogenic organisms.

Because FcγR expression is restricted predominantly to cells of the innate immune system, and many of the ligands for SAP are concentrated at sites of tissue injury, we predicted that SAP binding to ligands might affect innate immune cell activation events in a localized fashion and thereby potentially modulate the innate injury response. Despite extensive characterization of SAP in vitro (13,15–17), its potential participation in natural regulation of the innate injury response has only recently been appreciated (10,29–32). Pilling *et al.* first demonstrated that SAP could suppress the differentiation of monocytes into fibrocytes, a monocyte cell lineage implicated in fibrotic disease of the lung and other organs (29). They subsequently showed that purified rat SAP could suppress development of lung fibrosis in the bleomycin model (30), which correlated with reduced fibrocyte numbers within the lung tissue. However, fibrocytes play no obvious role in the development of fibrosis of the kidney (33); therefore, we wished to determine whether SAP would have an antifibrotic effect in this tissue setting and, if so, what mechanisms mediated its biologic effect.

# RESULTS

## Systemic administration of human SAP inhibits fibrosis in the kidney

Mice underwent unilateral ureteric obstruction (UUO) surgery to generate mechanical injury to the kidney, which results in a rapid, highly reproducible interstitial fibrosis independent of T and B lymphocytes (34). Human SAP (hSAP) or human serumalbumin (HSA) as a control was administered every 48 hours by intraperitoneal injection. hSAP specifically inhibited the development of fibrosis at both day 7 and day 14 (Fig. 1, A to C). hSAP was next administered to mice containing the *Coll1a1-GFP* transgene (*Coll-GFP*) that had undergone UUO surgery. Green fluorescent protein (GFP) expression by the kidney, indicative of myofibroblast activation, was markedly reduced by hSAP relative to HSA control (Fig. 1, A, D, and E) (33). Cohorts of mice with UUO kidney disease were also treated with low-dose and high-dose hSAP at different time intervals (Fig. 1F), showing that the effect of hSAP was dose-dependent. hSAP injections had no effect on the total number of α smooth muscle actin–positive ($\alpha SMA^+$) fibroblasts (Fig. 1, G and H); rather, the proportion of $\alpha SMA^+$ fibroblasts that expressed *Coll-GFP* was decreased by hSAP treatment (Fig. 1G). In addition, the extent of macrophage infiltration measured in tissue sections was unaffected by hSAP (Fig. 1H).

To confirm the broad antifibrotic effects of hSAP in kidney injury, we induced a second model of kidney fibrosis, the unilateral ischemia reperfusion injury (IRI) model. In this model, acute injury to the kidney is followed by repair, but nevertheless, significant fibrosis ensues (35). hSAP was administered after kidney IRI and the extent of fibrosis was determined at days 7 and 15. Similar to data in the UUO model, the extent of fibrosis was markedly decreased at both time points (Fig. 2, A to C), but the number of interstitial macrophages was unaffected (HSA, 8.9 ± 2.0% versus hSAP, 7.4 ± 1.6%; area of F4/80 stain on day 15).

Together these data indicate that fibroblasts are present in similar numbers after hSAP treatment, but that they show down-regulated fibrotic collagen gene transcription and collagen protein deposition, thereby identifying hSAP as a natural inhibitor of fibrosis during injury of the kidney. Other studies have identified SAP administration as anti-fibrotic in injury to lung and heart, supporting a generalized role for SAP in inhibition of fibrosis progression (30,32); however, in lung and heart, the antifibrotic effects of SAP correlated with decreased recruitment and/or activation of fibrocytes, myeloid lineage cells that generate collagen matrix directly. In recent comprehensive studies of fibrocytes in kidney fibrosis models using *Coll-GFP* reporter mice, fibrocytes made no significant contribution to fibrosis (33). Although specific culture of mouse monocytes in vitro readily induced fibrocyte morphology that was inhibited equivalently by human and mouse SAP (fig. S1), fibrocytes were rarely identified in diseased kidneys treated with HSA despite significant fibrosis progression (Fig. 1), confirming that fibrocytes do not contribute to kidney fibrosis. Therefore, we wished to determine what mechanisms mediated the biologic effect of hSAP in the kidney.

Many of the reported ligands for SAP, including components of cell debris, are concentrated at sites of tissue injury, and SAP staining is increased in injured skin after systemic administration (36). We tested whether systemically administered hSAP selectively localized to injured kidneys. We detected a marked increase of hSAP specifically in the injured kidney in both models of injury (Fig. 2, D to F). This retained hSAP was predominantly associated with apoptotic and necrotic cells (Fig. 2E), and many of the hSAP-stained cell debris were inside recruited macrophages (Fig. 2E).

## Kidney disease in humans correlates with reduced SAP concentrations

The studies in mice revealed that not only was hSAP antifibrotic, but that hSAP was deposited selectively in the injured kidney. In this sense, hSAP may share similarities with the

complement proteins that can be "consumed" at sites of inflammation, resulting in depressed plasma concentrations. That dosed hSAP ameliorates fibrosis and systemic administration increases hSAP deposition in the kidney also suggest that injury states might represent SAP deficiency. To test this, plasma hSAP concentrations were studied in a cohort of patients with chronic kidney diseases (fig. S2A). Patients with more severe kidney disease had significantly lower concentrations of hSAP in plasma relative to that of patients with mild kidney diseases and normal function, and there was a correlation between plasma hSAP concentration and loss of kidney function (fig. S2, B and C). Patients with more active kidney disease, indicated by an albumin leak of >300 mg a day from the kidney into the urine, also had lower hSAP concentrations (fig. S2D). Because lower plasma hSAP concentrations in patients with more severe kidney disease could be interpreted as either consumption of hSAP in the kidney or leak of hSAP into the urine, kidneys from patients with kidney injury were labeled for deposition of hSAP. These kidney sections also showed increased deposition of hSAP (fig. S2E), consistent with our findings in mice and in keeping with the hypothesis of SAP consumption by injured tissues.

## Human SAP binds directly to monocytes and macrophages, but not to fibroblasts

We next studied the effect of hSAP on fibroblasts, monocytes, and macrophages, using fluorescently labeled and functionally specific hSAP (hSAP conjugates with Alexa 594 or Alexa 488: SAP-594 or SAP-488) and similarly labeled HSA as control (fig. S3A). Primary cell cultures of kidney fibroblasts were established from kidneys of *Coll-GFP* mice on 7 days after UUO but did not bind to SAP-594 (Fig. 3A). Furthermore, when these fibroblasts were cultured inmedium containing hSAP but no other serum proteins or in medium containing 0.1% albumin, hSAP had no effect on collagen 1a1 promoter activity (Fig. 3B), suggesting that hSAP does not exert its in vivo antifibrotic effects on kidney fibroblasts directly.

Human SAP was reported to bind to FcγRs in indirect binding studies (21–23). Although mouse kidney fibroblasts do not express FcγRs (fig. S3C), monocytes and macrophages do (figs. S3D and S4, A and B). Human monocytes ($CD11b^{high}$) selectively bound SAP-488, whereas lymphocytes ($CD11b^{low}$) did not (Fig. 3, C and D). Mature purified mouse bone marrow monocytes (BMMs) avidly bound SAP-488 (Fig. 3E). Similarly, peripheral blood monocytes (PBMos) from mice taken 7 days after UUO surgery bound SAP-488 avidly (Fig. 3G) and with binding similar to that observed for human peripheral blood mononuclear cells (PBMCs) (Fig. 3C). By contrast, the majority of mouse PBMos from healthy mice did not bind hSAP (Fig. 3F). Because SAP-488 also bound to primary cultures of macrophages (fig. S3D), we purified inflammatory kidney macrophages from day 3, day 7, and day 10 UUO kidneys. At each time point, SAP-488 selectively and specifically bound to CD11b+ kidney macrophages (Fig. 3H). Collectively these studies indicated that in mice, inflammatory monocytes held in bone marrow, those released into the circulation during kidney injury, and kidney inflammatory macrophages, all bind hSAP.

## FcγRs are up-regulated by monocytes and macrophages in the injured kidney

Our studies indicated that hSAP bound to inflammatory monocytes and macrophages, possibly through FcγRs (20,21). We therefore assessed monocytes and macrophages for murine FcγR (mFcγR) expression. Inflammatory monocytes residing in bone marrow or circulating as PBMos expressed high concentrations of mFcγRI and mFcγRIII, moderate concentrations of mFcγRIV, and low concentrations of mFcγRII (fig. S4A). By contrast, only a minority of normal monocytes expressed mFcγRI and none expressed mFcγRII. Inflammatory macrophages isolated from day 7 UUO kidney expressed increased concentrations of mFcγRI, II, III, and IV, compared with inflammatory monocytes (fig. S4B), and distinct populations of kidney macrophages were identified based on levels of mFcγR expression.

### Human SAP binds to FcγRs

Previously published studies suggested hSAP binds to human FcγRs (hFcγRs) (20–23). However, no study has compared all four mFcγRs and the effect of the common FcRγ-chain on binding activity. We generated mouse fibroblast (3T3) cell lines exclusively expressing mFcγRI ± FcRγ, mFcγRII, mFcγRIII ± FcRγ, or mFcγRIV ± FcRγ (Fig. 3I). Control and receptor-expressing cells were incubated with SAP-488 at physiological concentrations and were assessed for specific binding (Fig. 3I). 3T3-mFcγRI cells alone did not bind SAP-488, but when coexpressed with FcRγ, binding activity was detected. 3T3-mFcγRII also bound SAP-488, albeit with substantially lower binding activity than the other receptors. 3T3-mFcγRIII cells and 3T3-mFcγRIV cells exhibited binding activity to SAP-488 that was also enhanced by coexpression of FcRγ (Fig. 3I and fig. S4C), and 3T3-mFcγRIV cells exhibited the greatest shift in SAP binding. Thus, hSAP has the capacity to bind all mouse FcγRs with a relative rank order of mFcγRIV > mFcγRIII ≥ mFcγRI > mFcγRII.

To characterize the direct association of hSAP protein with the hFcγR, using label-free surface plasmon resonance (Biacore), we studied the binding affinity of hSAP for all forms of hFcγRs (Fig. 3, J to L, fig. S4, and Table 1). In contrast to a recent publication (20), we did not observe specific binding of hFcγRs to hSAP when hSAP was directly coupled to the dextran surface, using the standard amine coupling procedure (fig. S4D). When the orientation was reversed and hFcγRs were coupled to the chip surface via amine coupling, binding to immunoglobulin G (IgG) was readily detected (Fig. 3J, upper panel), but there was no specific binding of hSAP to hFcγRs in this orientation either (Fig. 3J, lower panel).

SAP was reported to promote phagocytosis through coupling $Ca^{2+}$-dependent binding and opsonization of ligands to FcγR-mediated cell recognition (21–23). Therefore, we investigated whether hSAP would specifically bind hFcγRs if the hSAP was first oriented on a $Ca^{2+}$-dependent ligand. SAP recognizes several glycosaminoglycans as $Ca^{2+}$-dependent ligands, and dextran sulfate can competitively inhibit $Ca^{2+}$-dependent self-association of SAP (37). We tested whether hSAP would specifically bind to the dextran surface of the CM5 chip in a $Ca^{2+}$-dependent manner in the absence of amine-coupling reagents. We found that hSAP readily bound to the CM5 chip dextran surface and could be removed by 10 mM EDTA (Fig. 3K). To stabilize the oriented hSAP for subsequent binding to FcγRs, we followed hSAP-dextran association with a brief amine coupling pulse, yielding an oriented and highly-stable hSAP surface. Subsequent investigation of each hFcγR showed specific and high-affinity association of hSAP with most forms of hFcγRs, in the following order of affinity: hFcγRIIA ~ hFcγRIII > hFcγRI ≫ hFcγRIIB (Fig. 3L, fig. S4E, and Table 1). Therefore, although there are some differences between mouse and human specificities, in both species SAP preferentially binds to the immuno-receptor tyrosine–based activation motif (ITAM)–containing activating FcγRs, rather than the immunotyrosine-inhibitory motif (ITIM)–containing inhibitory mFcγRII (mouse) or hFcγRIIB (human). The fact that both human and mouse lymphocytes and NK (natural killer) cells express FcγRIII isoforms, but the predominant binding leukocyte in both species is the monocyte, indicates that cell surface expression alone is not sufficient for binding and that FcγRIII expression and binding to hSAP are not linearly related. Further, our biochemical studies suggest that hSAP only binds to hFcγRs with high affinity once hSAP is bound to a ligand (Fig. 3, J to L, and fig. S4E), such as would occur when SAP is bound to apoptotic and necrotic tissue at an injury site or when such debris is released into circulation. hSAP did not bind to 3T3-FcγR cell lines in the absence of bovine serum albumin (BSA) (a low-affinity SAP ligand). This regulated receptor preference could be important in SAP function by localizing SAP activity to sites of damaged tissue exposure, and suggests that SAP is a soluble danger-associated molecular pattern receptor (DAMP).

### Development of fibrosis in the kidney is dependent on monocytes/macrophages

Because hSAP bound selectively to monocyte lineage cells and FcγRs, yet was antifibrotic in the absence of fibrocytes, we explored a possible role for monocytes/macrophages in the progression of kidney fibrosis by paracrine mechanisms. Using diphtheria toxin (DT) to induce conditional ablation of monocytes/macrophages in the *Cd11b-DTR* mouse (12,38) from day 4 to day 7 resulted in a significant decrease in both fibrosis and monocyte/macrophage accumulation on day 7 (Fig. 4, C and D). In another cohort, kidneys were assessed at day 10 (Fig. 4, A and E) after DT administration on days 7 to 10. As expected there was a high level of ablation of monocytes in blood and of kidney macrophages (Fig. 4, A to C). Collagen accumulation was measured morphometrically by staining with Sirius red (Fig. 4, A and E), and fibrosis was markedly reduced at both day 7 and day 10 compared with vehicle-treated mice. In previous studies we have confirmed that DT has no direct effect on fibroblasts from *CD11b-DTR* mice and that these mice retain the normal complement of neutrophils (38). These findings are consistent with a paracrine role for macrophages in fibrosis progression.

### Human SAP triggers an anti-inflammatory signature in infiltrating macrophages

Because hSAP was predominantly detected bound to dead cells and debris in vivo (Fig. 2, D to G, and fig. S2), we hypothesized that hSAP opsonizes apoptotic cells, permitting FcγR-dependent clearance by macrophages as opposed to clearance via other receptors, and that this method of clearance may affect activation. First, we confirmed the binding of hSAP to cells undergoing UV-mediated apoptosis (Fig. 5A). Whereas there was little binding to healthy cultured human lymphocytes, there was progressive and striking binding of hSAP to lymphocytes early in the process of apoptosis. These studies suggested that hSAP-opsonized apoptotic cells would preferentially bind FcγRs. To test this, we incubated 3T3 cell lines expressing single mFcγRs with hSAP-opsonized or unopsonized apoptotic mouse lymphocytes and assessed the cell lines by flow cytometry for phagocytosis using established phagocytosis protocols (39). There was little difference in phagocytosis of hSAP-opsonized versus unopsonized apoptotic cells by cell lines expressing mFcγRII or mFcγRI (Fig. 5B). However, hSAP-opsonized apoptotic cells were more avidly phagocytosed by mFcγRIII- and mFcγRIV-expressing cell lines, implicating these two receptors in hSAP-mediated inhibition of fibrosis.

The leukocyte cell surface marker Ly6C labels subpopulations of circulating monocytes (40). Inflammatory monocytes that are selectively recruited to inflamed sites express high concentrations of Ly6C ($Ly6C^{high}$) and hSAP selectively bound to $Ly6C^{high}$ monocytes (Fig. 3, E to G, and fig. S5). To explore further the role of FcγR-mediated phagocytosis of apoptotic cells, mature BMMs that have high concentrations of Ly6C and express only the activating FcγRs (figs. S4, A and B, and fig. S5), were purified, incubated with unopsonized or hSAP-opsonized apoptotic cells, and coactivated with interferon-γ (IFN-γ) or immobilized IgG (iIgG) (Fig. 5C). Twenty-four hours later, hSAP-opsonized apoptotic cells had potently inhibited the activation of monocytes compared with unopsonized apoptotic cells. In these experiments, monocytes generated no detectable Il-6, Il-12, or *Pdgfb*, and hSAP opsonization had no effect on *Tgfb* transcript concentrations.

To study the functional consequences of hSAP opsonization and macrophage phagocytosis in vivo in the progression of kidney fibrosis, we purified kidney macrophages from day 7 UUO diseased kidney of mice treated with either HSA or hSAP by fluorescence-activated cell sorting (FACS) and measured messenger RNA (mRNA) transcript levels by branched-chain DNA (bDNA) amplification or quantitative polymerase chain reaction (Q-PCR). The leukocyte cell surface marker Ly6C also labels three discrete subpopulations of kidney macrophages designated $Ly6C^{high}$, $Ly6C^{int}$, and $Ly6C^{low}$ (fig. S5), which separates macrophages into M1 type ($Ly6C^{high}$) and M2 type ($Ly6C^{low}$) functions. $Ly6C^{int}$ cells represent both $Ly6C^{high}$ cells transitioning to $Ly6C^{low}$ cells and the resident macrophage population. As expected, the three

populations of kidney macrophages differed greatly in transcript profiles. The Ly6C$^{high}$ macrophages were activated and transcribed high concentrations of M1 type transcripts including *Mip2a* and *Il-1*β, and the Ly6C$^{low}$ macrophages transcribed high concentrations of M2-type transcripts including *Ccl17* and *Ccl22*. Systemic administration of hSAP inhibited transcription of both M1-type and M2-type cytokines (Fig. 5D), indicating that hSAP functions to buffer activation of inflammatory monocytes and macrophages in vivo. In addition, transcripts of the anti-inflammatory and antifibrotic cytokine *Il-10* were markedly up-regulated in all three populations of kidney macrophages (Fig. 5D). In whole kidney 10 days after UUO, IL-10 protein was increased selectively in mice treated with hSAP (Fig. 5E), confirming the transcriptional studies. Furthermore, human monocytes cultured with hSAP robustly generated IL-10 protein (Fig. 5F), collectively suggesting local IL-10 production by inflammatory macrophages may be central to the efficacy of hSAP.

## Fibrosis progression is dependent on activating FcγRs and IL-10

Our data implicate macrophage FcγRs in the progression of kidney fibrosis. To examine the role of these receptors further, we induced UUO in kidneys from mice lacking FcRγ (FcR$\gamma^{-/-}$). Leukocytes from these mice have no cell surface expression of activating receptors FcγRI, III, and IV. After 10 days of UUO, the extent of fibrosis in FcR$\gamma^{-/-}$ and strain-matched wild-type control mice was compared. Fibrosis was significantly reduced in mice without FcRγ (Fig. 6A). To understand whether there was any role for the inhibitory receptor FcγRII in this process, FcγRII$^{-/-}$ mice had UUO surgery and were compared with strain-matched controls. The absence of FcγRII resulted in enhanced accumulation of collagen matrix relative to strain-matched controls (Fig. 6B). However, mice lacking only FcγRIII that underwent UUO surgery developed fibrosis comparable with that of wild-type controls (Fig. 6C), indicating a negligible or redundant role for FcγRIII function in kidney fibrosis. These studies suggested that ITAM-bearing FcγRs played a positive role in leukocyte activation. Nevertheless, when hSAP was given to FcR$\gamma^{-/-}$ mice or wild-type controls with UUO-induced kidney fibrosis, the antifibrotic effect of hSAP was markedly attenuated in the absence of activating FcγRs (Fig. 6D), confirming the in vivo role of activating FcγRs in hSAP-dependent signaling. To explore the role of activating FcγRs further, monocytes from FcR$\gamma^{-/-}$ or wild-type mice were incubated with hSAP and coactivated with immobilized IgG, IFN-γ, the TLR4 (Toll-like receptor 4) ligand LPS, or combinations of these activating stimuli. Strikingly, FcR$\gamma^{-/-}$ monocytes were resistant to activation by all pro-inflammatory cytokines (Fig. 6E). Furthermore, hSAP had no effect on inhibition of cytokine production by FcR$\gamma^{-/-}$ monocytes, in distinction from wild-type monocytes (Figs. 5 and 6E), indicating that hSAP signals through activating FcγRs in monocytes and that activating FcγRs play broad roles in regulating monocyte activation.

Soluble immunoglobulins are readily detected in injured but not in healthy tissues. Whereas monocytes are susceptible to activation by complexed or immobilized IgG, but not soluble IgG, mature primary macrophages are susceptible to activation by soluble IgG (fig. S6A), particularly after IFN-γ incubation. Incubation with IFN-γ had no effect on FcγR expression. Strikingly, hSAP (in BSA containing serum-free buffer) inhibited TNFα (tumor necrosis factor–α) release triggered by soluble IgG (fig. S5B).

Although little IL-10 was detected in fibrotic kidney after UUO in the absence of SAP injections, it was synthesized by macrophages after FcγR ligation by SAP (Fig. 5, D to F). As expected, mice deficient in IL-10 had similar levels of fibrosis after UUO-induced injury of the kidney (Fig. 6F). However, hSAP no longer inhibited the progression of fibrosis in IL-10–deficient mice. These genetic studies implicate IL-10 release by macrophages in the kidney in the mechanism of action of hSAP. To test whether IL-10 alone could inhibit fibrosis, using adenoviruses, we overexpressed IL-10 systemically in mice. Systemic IL-10 expression in plasma at the time of ureteral ligation surgery was confirmed (38.0 ± 6.7 ng/ml [Ad-IL-10]

versus 4.9 ± 2.3 ng/ml [AdMock] versus 0 ± 0 ng/ml [no virus]) and fibrosis progression was markedly inhibited (Fig. 6G). Whereas ligation of the IL-10 receptor onmacrophages inhibits activation, IL-10 can also directly inhibit collagen production by myofibroblasts, which also express the IL-10 receptor (Fig. 6H).

## DISCUSSION

These studies identify SAP as a natural inhibitor of fibrosis during inflammatory injury of the kidney. Moreover they show a potential role for hSAP as a therapeutic compound in the treatment of inflammation associated with fibrosis. We identified previously unknown mechanisms of action of hSAP in regulating anti-inflammatory clearance of apoptotic and necrotic cell debris in injured tissues and down-regulating activation of monocytes and macrophages that direct fibrosis, and identified hSAP as a soluble DAMP receptor, coupling injury to recognition by activating FcγRs (Fig. 7).

The most obvious cell types to bind hSAP and mediate an antifibrotic effect are the fibroblast and fibrocyte. However, our in vivo and in vitro studies provide no supportive data for a direct interaction between fibroblasts and hSAP in the kidney. Further, although we did confirm that mouse monocyte culture can induce differentiation into fibrocytes, and that both hSAP and mSAP inhibit this differentiation with similar dose titrations (fig. S1A), we did not find any evidence to support a role for fibrocytes in contributing to the kidney myofibroblast pool (fig. S1, B and C). Instead, our results highlight the importance of the monocyte/macrophage in mediating SAP's antifibrotic effect within the kidney.

Previous studies have identified binding ligands for hSAP, including apoptotic and necrotic cells and binding receptors for hSAP including FcγRs (21–24,26). Our studies confirm that hSAP rapidly recognizes both early and late apoptotic cells and show that in vivo administration of hSAP results in deposition of hSAP in the injured organ with binding to both dead cells and interstitial macrophages in vivo. hSAP behaves similarly to complement components in that it opsonizes dead cells and binds specifically to receptors on macrophages. Moreover, the recruitment of hSAP to the site of injury may explain why plasma concentrations of hSAP fall in patients with inflammatory diseases of the kidney; the fall is most likely due to consumption.

Our studies independently confirm with the use of previously undescribed methods that hSAP is a ligand for FcγRs. Although in the mouse it binds to all FcγRs, hSAP showed preference for the activating receptors (RIV, RI, and RIII) over the inhibitory receptor (RII), and a similar preference was shown in our studies with human receptors where little binding activity was observed for hFcγRIIB, the human inhibitory receptor, but hSAP has the greatest affinity for the activating receptors hFcγRIIA and hFcγRIII. We also demonstrated that high-affinity binding of hSAP to hFcγR occurs upon $Ca^{2+}$-dependent ligand binding. This ligand-dependent receptor preference may be important in SAP function by localizing SAP activity selectively to sites of damaged tissue exposure and identifying SAP as a soluble DAMP receptor. On murine monocytes and inflammatory kidney macrophages, mFcγRII represents only a small proportion of the target FcγRs for hSAP. In addition, hSAP-opsonized apoptotic cells are preferentially recognized by mFcγRIII and mFcγRIV, not mFcγRII, which suggests that hSAP in rodents also likely functions by binding to the activating FcγRs.

The prevailing model of FcγR function is that activating receptors, mFcγRI, III, and IV (hFcγRI, IIA, and III) activate leukocytes and that mFcγRII (hFcγRIIB) inhibits activation. Our data, however, indicate that ligation of mFcγRIV and/or mFcγRIII by hSAP or hFcγRIIA and/or hFcγRIII results in potent inhibition of leukocyte activation, pointing to more complex signaling in monocytes/macrophages induced by ITAM signaling through activating FcγRs than has previously been appreciated. One possible mechanism is that in vivo, SAP effectively

competes for IgG binding to mFcγRIV and mFcγRI without inducing a productive activating signal, although at the same time allowing IgG to ligate mFcγRII, thereby indirectly amplifying the negative regulatory activity of mFcγRII. Alternatively, ligation of activating FcγR by SAP may induce an anergic signaling pathway in monocytes/macrophages similar to the effect of partial agonist peptides on TCR signaling. Presentation of such altered peptide ligands results in recruitment but not activation of the Syk-family kinase ZAP-70 (41,42). SAP-mediated inhibition of monocyte to fibrocyte differentiation is dependent on Src family kinase signaling, but not Syk family kinase signaling (31). Further studies will be required to determine whether hSAP ligation of activating FcγRs results in a distinct intracellular signaling signature compared with ligation by IgGs.

In dissecting the mechanism of action of hSAP, we have determined that FcγRs participate in fibrosis progression. Because FcRγ$^{-/-}$ monocytes are hypoactivated by a range of stimuli, FcγRI, III, and IV may help to regulate leukocyte activation. Thus, activating FcγRs may be generally important in macrophage activation during sterile inflammation and suggest that additional therapies targeting FcγRs could also regulate the progression of fibrosis.

In both human and mouse macrophages, inhibition of activation by hSAP is at least in part due to release of IL-10 (Fig. 7). This immunomodulatory cytokine inhibits macrophage activation, and the studies presented here implicate local IL-10 release in both indirect (deactivation of macrophages, which results in down-regulation of paracrine signals that activate myofibroblasts) and direct (down-regulation of collagen transcription in myofibroblasts) actions on collagen-producing cells. IL-10 has a short circulating half-life, limiting its systemic therapeutic application. In addition, it stimulates B cell proliferation and may be deleterious if administered systemically. Because hSAP administration results in local release of IL-10 at the site of injury, potential systemic side effects of IL-10 may be avoided, and hSAP modulation of monocyte/macrophage production of IL-10 may result in longer exposure of the tissue to the regulatory capacity of this cytokine than its systemic application could accomplish.

That administration of hSAP promotes anti-inflammatory responses in our studies indicates that inflammation in the kidney may represent a local state of functional deficiency in SAP. Alternatively, consumption of hSAP through recruitment to the site of injury may explain why plasma concentrations fall in patients with inflammatory kidney diseases. SAP may be tonically produced by the liver in health as a mechanism to limit leukocyte activation except in overwhelming circumstances. Our data identify hSAP as a DAMP receptor that then serves as a ligand for activating FcγRs, triggering anti-inflammatory clearance of apoptotic and necrotic cell debris in the injured tissues and down-regulating activation of monocytes and macrophages. Moreover, they demonstrate a strong potential for hSAP as a therapeutic compound in the treatment of inflammation and fibrosis. A recombinant form of hSAP, PRM-151, has been produced by Promedior, Inc., and is currently being tested in a phase 1 single ascending dose clinical trial to assess safety and pharmacokinetics in healthy volunteers (Promedior press release). We are hopeful that subsequent testing in patients with active fibrotic disease will determine whether the strong therapeutic potential indicated here can be translated into appropriate clinical practice.

## MATERIALS AND METHODS

### Mouse breeding and genotyping

Wild-type C57BL/6 mice were from Charles River Laboratories. *Cd11b-DTR* mice (FVB/N) were generated and maintained as previously described (12). *Coll-GFP* transgenic mice were generated on the C57BL6 background and validated as previously described (33). The presence of *CD11b-DTR* was confirmed by genomic DNA PCR with the following primers: 5′-TTCCACTGGATCTACGGACC-3′, 5′-TGTCGGCCATGATATAGACG-3′. FcRγ-chain$^{-/-}$

mice and strain-matched controls (B6;129P2-Fcer1gtm1Rav/J-B6;129P2-Fcer1gtm1Rav/J) were from Taconic Laboratories (43); FcγRII$^{-/-}$ mice and strain-matched controls (B6;129S4-*Fcgr2b*$^{tm1Ttk}$/J-B6129SF2/J) (44) and FcγRIII$^{-/-}$ mice were from Jackson Laboratories (B6.129P2-Fcgr3tm1Sjv/J- C57BL/6J) (45); and IL-10$^{-/-}$ (B6.129P2-*Il-10*$^{tm1Cgn}$/*J*) mice were from Jackson Laboratories Genotyping of the mouse strains was carried out according to protocols available at the Jackson Laboratory Web site.

## Mouse models of fibrosis

Adult (12 to 20 weeks) male mice [C57BL6, *Coll-GFP*, *CD11b-DTR*, *FcγRII*$^{-/-}$, *FcγRIII*$^{-/-}$, FcRγ-chain$^{-/-}$, IL-10$^{-/-}$ and age-matched controls ($n \geq 5$ per group)] were anesthetized with ketamine-xylazine [100/10 mg/kg intraperitoneally (ip)] before surgery. UUO surgery was carried out as previously described (46), and kidneys, blood, spleen, and bone marrow were collected on days 0, 7, 10, or 14. Renal unilateral IRI was performed as previously described (35), and tissues were harvested on day 7 or day 15 after IRI. In some experiments, hSAP (20 μg/g) was administered intraperitoneally or intravenously on alternate days or daily from day 0 of disease induction until harvesting of organs. HSA (20 μg/g) was administered to separate cohorts of mice as a control protein. In experiments with macrophage ablation, 25 ng/g DT (List Biological Laboratories Inc.) in 100 μl or vehicle was given on day 4 and day 6 or day 7 and day 9 by tail vein injection ($n \geq 5$ per group); separate cohorts of mice received equal volumes of vehicle. Kidneys and blood were collected on day 7 or day 10 (12, 33). In experiments using mutant mice, age, weight, sex, and strain-matched wild type mice were used as controls, treated identically, and blinded to the surgeon. In some experiments adenoviruses [$5 \times 10^8$ plaque-forming units (PFU)] were given to mice 3 days before surgery by tail vein injection in 200 μl of vehicle. Plasma concentrations of IL-10 were quantified by ELISA (enzyme-linked immunosorbent assay) on day 0 and day 10 of kidney injury. All surgical procedures were carried out in accordance with Protocols approved by the Harvard Animal Resources and Comparative Medicine Committee.

## Tissue preparation and histology

Mouse tissues were prepared, fixed, stored, and sectioned as previously described (47). Periodic acid Schiff staining was performed on paraffin sections using standard methods. Primary antibodies against the following proteins were used for immunolabeling: αSMA-Cy3 (1:200, clone 1A4, Sigma), CD11b (1:200, eBioscience), F4/80 (1:200, Caltag), CD45 [fluorescein isothiocyanate (FITC)-conjugated 1:400, EBioscience] CD34 (1:200, Pharmingen), and collagen III (1:400, Southern Biotech). Fluorescence-conjugated affinity-purified secondary antibody labeling (1:400-1:800, Jackson), mounting with Vectashield/DAPI (4′,6-diamidino-2-phenylindole), image capture, and processing were carried out as previously described (39,47). For morphometric analysis of collagen fibril staining, deparaffinized sections were stained with 0.1% picrosirius red or trichrome stain (12). For morphometric analyses of collagen III deposition and macrophage infiltration (F4/80 staining), deparaffinized sections or air-dried PLP (periodate-lysine-paraformaldehyde)-fixed cryosections were incubated with primary antibody, followed by biotinylated secondary antibodies (DAKO) amplified with Vectastain Elite ABC peroxidase staining kit, and the final stain was generated with DAB (diaminobenzidine) as previously described (12). For morphometric analysis of Coll1a1-GFP, cryosections of kidneys from *Coll-GFP* mice were mounted with Vectashield, and the digital images were captured at 200× magnification with a Nikon TE2000 microscope, a Coolsnap digital camera, and IP Lab software (46). For quantification of αSMA cells, CD11b cells, orCD45$^+$,CD34$^+$ cells, counting of random sections was carried out as previously described (29). In brief, sections were co-labeled with DAPI, and *Coll1a1-GFP*–positive cells were identified by blue and green nuclear colocalization; αSMA-positive cells were identified by greater than 75% of the cell area immediately surrounding the nuclei (detected by DAPI) staining positive with Cy3

fluorescence indicative of the antigen expression. Low-power field images were captured at 100× magnification, and high-power field images at 400×.

To identify hSAP in kidney sections, tissue sections were deparaffinized, rehydrated, and boiled in citric buffer for 15 min for epitope retrieval. After rinsing in phosphate-buffered saline (PBS), the sections were incubated with 1% normal rabbit serum (30 min) then incubated overnight at 4°C with rabbit antibody against hSAP (1:300 dilution, Abcam, cat. no. ab 45151). After washing with PBS, the sections were then incubated for 20 min at room temperature with Alexa Fluor 488–labeled goat secondary antibody against rabbit (1:500 dilution; Invitrogen, cat. no.A11008).After washing with PBS, the sections were mounted with antifade mounting medium containing DAPI. Morphometry was performed as previously described. To co-label hSAP and macrophages, PLP-fixed cryosections were prepared and rabbit antibodies against hSAP were applied in 10% goat serum (as above but without antigen retrieval), followed by goat Cy3-conjugated secondary antibodies against rabbit, followed by antibodies against CD11b-FITC, with methods previously described (33), and confocal images were captured with a Nikon C1D-Eclipse confocal microscope.

## Single-cell preparation from blood, bone marrow, and kidney

Mouse blood (500 μl) was collected from the inferior vena cava into sodium citrate (0.38%).Mice were flushed with ice-cold PBS to remove remaining blood, and kidneys and bone marrow were harvested as previously described (33). PBMCs were isolated from citrated whole blood with Ficoll-Paque PLUS (GE Healthcare). Single cells were resuspended in FACS buffer (33,47) after centrifugation. The kidney was decapsulated, diced, incubated (37°C, 30 min) with liberase (0.5 mg/ml, Roche) and deoxyribonuclease (100 U/ml, Roche) in HBSS (Hanks' balanced salt solution), then resuspended in 10 ml of FACS buffer or PBS/1% BSA, and cells were filtered (40 μm). In some cases, leukocyte enrichment was carried out by resuspending the single-cell suspension in PBS, then overlaying it on a discontinuous Percoll gradient (33%, 66% in PBS), followed by centrifugation (20 min, 620*g*). Mouse bone marrow was flushed out of the femur, filtered through a 70-μm cell strainer, and resuspended in FACS buffer or PBS/1% BSA.

Mouse PBMos were purified from PBMCs by FACS sorting CD11b+, forward scatter (FSC) high, side scatter (SSC) low cells (FACSAria). Human monocytes were purified from 20 ml of citrated whole blood from healthy normal volunteers. PBMCs were separated by Ficoll-Paque PLUS (GE Healthcare) density centrifugation. Mouse BMMs were purified from erythrocyte-depleted bone marrow by negative selection with MACS beads (Miltenyi Biotech). In brief, bone marrow in buffer was incubated with phycoerythrin (PE)-conjugated antibodies against Ly6G, B220, and CD90. Anti-PE magnabeads were then incubated with the leukocytes and the whole incubation mixture was passed through a magnetic column. Nonadherent cells were washed through the column and tested for purity by flow cytometry. There was >90% depletion of CD90, B220, and LyG+ cells (not shown).

## Flow cytometric analysis

Single cells ($2 \times 10^5$) from kidney, PBMCs, or bone marrow were resuspended in FACS buffer (39) and incubated for 30 min at 4°C with antibodies against CD11b, CD16/32, F4/80 (APC-conjugated, eBioscience), CD64 (Alexa Fluor 647–conjugated, 1:200, BD Biosciences), and Ly6C (FITC-conjugated, 1:200, BD Biosciences) at 4°C in the presence of 2% mouse serum. Cells were washed three times with FACS wash buffer, then fixed in 200 μl of FACS buffer/1% PFA (paraformaldehyde), and analyzed with a BD FACSCalibur flow cytometer. Note that in C57Bl/6 mice, antibodies against CD16/32 recognize only CD16 (48). For detection of mFcγRII, specific antibody against Ly-17.2 (clone K9.361) (1:500, Sloan Kettering) (48) in 2% mouse serum was used, followed by FITC-conjugated, affinity purified, goat secondary

antibodies against mouse IgG (1:500, Jackson Immunoresearch). To detect mFcγRIV, clone 9G8.1 (1:800, Sloan Kettering)–specific antibody in 2% mouse serum was used (49), followed by PE-conjugated goat secondary antibodies against hamster IgG (BD Biosciences). In preliminary experiments, isotype controls followed by secondary antibodies showed no specific binding, and primary dilution was optimized. Specificity of antibodies was confirmed with 3T3 cell lines expressing single FcγRs (not shown). All studies were repeated at least three times and gave results comparable to those presented.

### Statistical analysis

Error bars represent SEM. One-way analysis of variance or *t* test was carried out with GraphPad Prizm (GraphPad Software).

## Supplementary Material

Refer to Web version on PubMed Central for supplementary material.

## REFERENCES AND NOTES


1. Sansonetti PJ. The innate signaling of dangers and the dangers of innate signaling. Nat. Immunol 2006;7:1237–1242. [PubMed: 17110939]
2. Eddy AA. Progression in chronic kidney disease. Adv. Chronic Kidney Dis 2005;12:353–365. [PubMed: 16198274]
3. Lupher ML Jr, Gallatin WM. Regulation of fibrosis by the immune system. Adv. Immunol 2006;89:245–288. [PubMed: 16682276]
4. Duffield JS. The inflammatory macrophage: A story of Jekyll and Hyde. Clin. Sci. (Lond.) 2003;104:27–38. [PubMed: 12519085]
5. Gordon S. Alternative activation of macrophages. Nat. Rev. Immunol 2003;3:23–35. [PubMed: 12511873]
6. Mantovani A, Sica A, Locati M. Macrophage polarization comes of age. Immunity 2005;23:344–346. [PubMed: 16226499]
7. Mantovani A, Sica A, Sozzani S, Allavena P, Vecchi A, Locati M. The chemokine system in diverse forms of macrophage activation and polarization. Trends Immunol 2004;25:677–686. [PubMed: 15530839]
8. Mantovani A, Sozzani S, Locati M, Allavena P, Sica A. Macrophage polarization: Tumor-associated macrophages as a paradigm for polarized M2 mononuclear phagocytes. Trends Immunol 2002;23:549–555. [PubMed: 12401408]
9. Gomperts BN, Strieter RM. Fibrocytes in lung disease. J. Leukoc. Biol 2007;82:449–456. [PubMed: 17550974]
10. Quan TE, Cowper S, Wu SP, Bockenstedt LK, Bucala R. Circulating fibrocytes: Collagen-secreting cells of the peripheral blood. Int. J. Biochem. Cell Biol 2004;36:598–606. [PubMed: 15010326]
11. Fallowfield JA, Mizuno M, Kendall TJ, Constandinou CM, Benyon RC, Duffield JS, Iredale JP. Scar-associated macrophages are a major source of hepatic matrix metalloproteinase-13 and facilitate the resolution of murine hepatic fibrosis. J. Immunol 2007;178:5288–5295. [PubMed: 17404313]
12. Duffield JS, Forbes SJ, Constandinou CM, Clay S, Partolina M, Vuthoori S, Wu S, Lang R, Iredale JP. Selective depletion of macrophages reveals distinct, opposing roles during liver injury and repair. J. Clin. Invest 2005;115:56–65. [PubMed: 15630444]
13. Mantovani A, Garlanda C, Doni A, Bottazzi B. Pentraxins in innate immunity: From C-reactive protein to the long pentraxin PTX3. J. Clin. Immunol 2008;28:1–13. [PubMed: 17828584]
14. Garlanda C, Bottazzi B, Bastone A, Mantovani A. Pentraxins at the crossroads between innate immunity, inflammation, matrix deposition, and female fertility. Annu. Rev. Immunol 2005;23:337–366. [PubMed: 15771574]
15. Gewurz H, Zhang XH, Lint TF. Structure and function of the pentraxins. Curr. Opin. Immunol 1995;7:54–64. [PubMed: 7772283]

16. Steel DM, Whitehead AS. The major acute phase reactants: C-reactive protein, serum amyloid P component and serum amyloid A protein. Immunol. Today 1994;15:81–88. [PubMed: 8155266]

17. Pepys MB, Tennent GA, Booth DR, Bellotti V, Lovat LB, Tan SY, Persey MR, Hutchinson WL, Booth SE, Madhoo S, Soutar AK, Hawkins PN, Van Zyl-Smit R, Campistol JM, Fraser PE, Radford SE, Robinson CV, Sunde M, Serpell LC, Blake CC. Molecular mechanisms of fibrillogenesis and the protective role of amyloid P component: Two possible avenues for therapy. Ciba Found. Symp 1996;199:73–81. [PubMed: 8915605]

18. Hutchinson WL, Hohenester E, Pepys MB. Human serum amyloid P component is a single uncomplexed pentamer in whole serum. Mol. Med 2000;6:482–493. [PubMed: 10972085]

19. Emsley J, White HE, O'Hara BP, Oliva G, Srinivasan N, Tickle IJ, Blundell TL, Pepys MB, Wood SP. Structure of pentameric human serum amyloid P component. Nature 1994;367:338–345. [PubMed: 8114934]

20. Lu J, Marnell LL, Marjon KD, Mold C, Du Clos TW, Sun PD. Structural recognition and functional activation of FcγR by innate pentraxins. Nature 2008;456:989–992. [PubMed: 19011614]

21. Bharadwaj D, Mold C, Markham E, Du Clos TW. Serum amyloid P component binds to Fcγ receptors and opsonizes particles for phagocytosis. J. Immunol 2001;166:6735–6741. [PubMed: 11359830]

22. Mold C, Baca R, Du Clos TW. Serum amyloid P component and C-reactive protein opsonize apoptotic cells for phagocytosis through Fcγ receptors. J. Autoimmun 2002;19:147–154. [PubMed: 12419285]

23. Mold C, Gresham HD, Du Clos TW. Serum amyloid P component and C-reactive protein mediate phagocytosis through murine FcγRs. J. Immunol 2001;166:1200–1205. [PubMed: 11145702]

24. Bijl M, Bootsma H, Van Der Geld Y, Limburg PC, Kallenberg CG, Van Rijswijk MH. Serum amyloid P component levels are not decreased in patients with systemic lupus erythematosus and do not rise during an acute phase reaction. Ann. Rheum. Dis 2004;63:831–835. [PubMed: 15194579]

25. Ciurana CL, Hack CE. Competitive binding of pentraxins and IgM to newly exposed epitopes on late apoptotic cells. Cell. Immunol 2006;239:14–21. [PubMed: 16643876]

26. Familian A, Zwart B, Huisman HG, Rensink I, Roem D, Hordijk PL, Aarden LA, Hack CE. Chromatin-independent binding of serum amyloid P component to apoptotic cells. J. Immunol 2001;167:647–654. [PubMed: 11441067]

27. Cathcart ES, Wollheim FA, Cohen AS. Plasma protein constituents of amyloid fibrils. J. Immunol 1967;99:376–385. [PubMed: 4166247]

28. Ashton AW, Boehm MK, Gallimore JR, Pepys MB, Perkins SJ. Pentameric and decameric structures in solution of serum amyloid P component by X-ray and neutron scattering and molecular modelling analyses. J. Mol. Biol 1997;272:408–422. [PubMed: 9325100]

29. Pilling D, Buckley CD, Salmon M, Gomer RH. Inhibition of fibrocyte differentiation by serum amyloid P. J. Immunol 2003;171:5537–5546. [PubMed: 14607961]

30. Pilling D, Roife D, Wang M, Ronkainen SD, Crawford JR, Travis EL, Gomer RH. Reduction of bleomycin-induced pulmonary fibrosis by serum amyloid P. J. Immunol 2007;179:4035–4044. [PubMed: 17785842]

31. Pilling D, Tucker NM, Gomer RH. Aggregated IgG inhibits the differentiation of human fibrocytes. J. Leukoc. Biol 2006;79:1242–1251. [PubMed: 16543402]

32. Haudek SB, Trial J, Xia Y, Gupta D, Pilling D, Entman ML. Fc receptor engagement mediates differentiation of cardiac fibroblast precursor cells. Proc. Natl. Acad. Sci. U.S.A 2008;105:10179–10184. [PubMed: 18632582]

33. Lin SL, Kisseleva T, Brenner DA, Duffield JS. Pericytes and perivascular fibroblasts are the primary source of collagen-producing cells in obstructive fibrosis of the kidney. Am. J. Pathol 2008;173:1617–1627. [PubMed: 19008372]

34. Shappell SB, Gurpinar T, Lechago J, Suki WN, Truong LD. Chronic obstructive uropathy in severe combined immunodeficient (SCID) mice: Lymphocyte infiltration is not required for progressive tubulointerstitial injury. J. Am. Soc. Nephrol 1998;9:1008–1017. [PubMed: 9621283]

35. Duffield JS, Hong S, Vaidya VS, Lu Y, Fredman G, Serhan CN, Bonventre JV. Resolvin D series and protectin D1 mitigate acute kidney injury. J. Immunol 2006;177:5902–5911. [PubMed: 17056514]

36. Naik-Mathuria B, Pilling D, Crawford JR, Gay AN, Smith CW, Gomer RH, Olutoye OO. Serum amyloid P inhibits dermal wound healing. Wound Repair Regen 2008;16:266–273. [PubMed: 18318811]
37. Hamazaki H. Calcium-dependent polymerization of human serum amyloid P component is inhibited by heparin and dextran sulfate. Biochim. Biophys. Acta 1989;998:231–235. [PubMed: 2478195]
38. Duffield JS, Tipping PG, Kipari T, Cailhier JF, Clay S, Lang R, Bonventre JV, Hughes J. Conditional ablation of macrophages halts progression of crescentic glomerulonephritis. Am. J. Pathol 2005;167:1207–1219. [PubMed: 16251406]
39. Ichimura T, Asseldonk EJ, Humphreys BD, Gunaratnam L, Duffield JS, Bonventre JV. Kidney injurymolecule-1 is a phosphatidylserine receptor that confers a phagocytic phenotype on epithelial cells. J. Clin. Invest 2008;118:1657–1668. [PubMed: 18414680]
40. Geissmann F, Jung S, Littman DR. Blood monocytes consist of two principal subsets with distinct migratory properties. Immunity 2003;19:71–82. [PubMed: 12871640]
41. Sloan-Lancaster J, Shaw AS, Rothbard JB, Allen PM. Partial T cell signaling: Altered phospho-ζ and lack of zap70 recruitment in APL-induced T cell anergy. Cell 1994;79:913–922. [PubMed: 8001128]
42. Madrenas J, Wange RL, Wang JL, Isakov N, Samelson LE, Germain RN. ζ phosphorylation without ZAP-70 activation induced by TCR antagonists or partial agonists. Science 1995;267:515–518. [PubMed: 7824949]
43. Takai T, Li M, Sylvestre D, Clynes R, Ravetch JV. FcR γ chain deletion results in pleiotrophic effector cell defects. Cell 1994;76:519–529. [PubMed: 8313472]
44. Takai T, Ono M, Hikida M, Ohmori H, Ravetch JV. Augmented humoral and anaphylactic responses in Fcγ RII-deficient mice. Nature 1996;379:346–349. [PubMed: 8552190]
45. Hazenbos WL, Gessner JE, Hofhuis FM, Kuipers H, Meyer D, Heijnen IA, Schmidt RE, Sandor M, Capel PJ, Daëron M, van de Winkel JG, Verbeek JS. Impaired IgG-dependent anaphylaxis and Arthus reaction in FcγRIII (CD16) deficient mice. Immunity 1996;5:181–188. [PubMed: 8769481]
46. Humphreys BD, Valerius MT, Kobayashi A, Mugford JW, Soeung S, Duffield JS, McMahon AP, Bonventre JV. Intrinsic epithelial cells repair the kidney after injury. Cell Stem Cell 2008;2:284–291. [PubMed: 18371453]
47. Duffield JS, Park KM, Hsiao LL, Kelley VR, Scadden DT, Ichimura T, Bonventre JV. Restoration of tubular epithelial cells during repair of the postischemic kidney occurs independently of bone marrow-derived stem cells. J. Clin. Invest 2005;115:1743–1755. [PubMed: 16007251]
48. Holmes KL, Palfree RG, Hammerling U, Morse HC III. Alleles of the Ly-17 alloantigen define polymorphisms of the murine IgG Fc receptor. Proc. Natl. Acad. Sci. U.S.A 1985;82:7706–7710. [PubMed: 3865190]
49. Nimmerjahn F, Bruhns P, Horiuchi K, Ravetch JV. FcγRIV: A novel FcR with distinct IgG subclass specificity. Immunity 2005;23:41–51. [PubMed: 16039578]


50. Acknowledgments: We thank D. Brenner, B.-L. Chiang and the Common Laboratory at National Taiwan University Hospital, D. Pilling, R. Gomer, D. Hesson, M. Kramer, L. Murray, M. Sayegh, D. Kozoriz, and S. Jogani for assistance or advice; L.-L. Hsiao, R. Jensen, and M. Lombardi for initial analysis of macrophage transcriptomes; and M. L. Hawes, B. A. Watkins, and E. G. Fey (Biomodels LLC) for technical assistance in some of the UUO experiments.Funding: Supported by NIH (grants DK73299, DK84077, and DK87389 to J.S.D.), Promedior Inc. (J.S.D.), American Society of Nephrology (Gottschalk Award), and an award from the National Taiwan Science Council (S.L.L.).

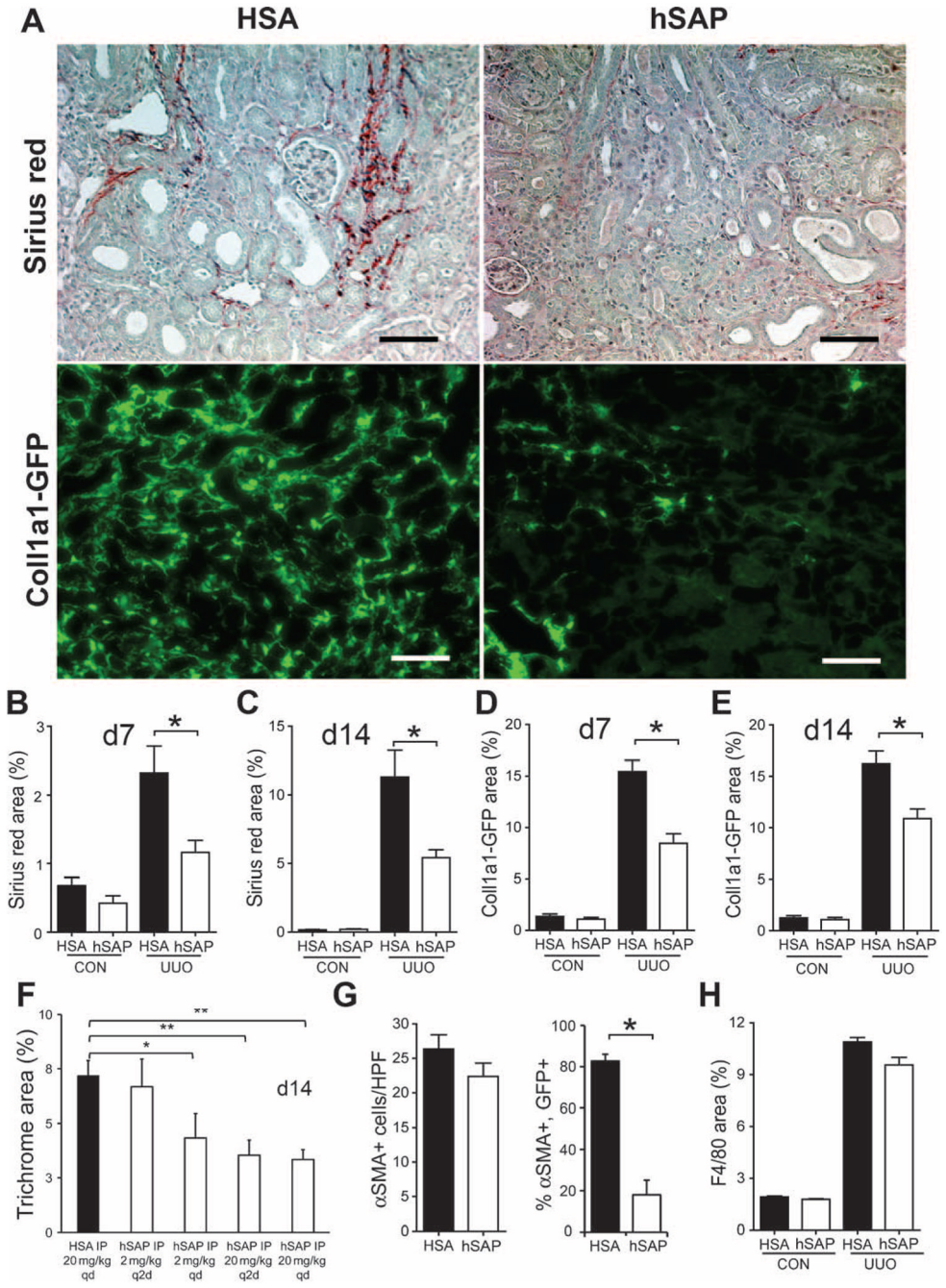


**Fig. 1.**

SAP inhibits kidney fibrosis after unilateral ureteral obstruction. (**A**) Photomicrograph of Sirius red stain or GFP immunofluorescence of day 14 UUO kidneys in Coll1a1-GFP mice treated with HSA or hSAP. Scale bar, 50 μm. (**B** and **C**) Morphometric quantification of Sirius red–stained area on (B) day 7 (d7) after UUO or (C) d14 after UUO in kidneys of mice treated with HSA or hSAP [20 mg/kg every 2 days (q2d), $n = 6$ per group]. CON, control. (**D** and **E**) Morphometric quantification of GFP area on (D) d7 after UUO or (E) d14 after UUO in kidneys of *Coll-GFP* mice treated with HSA or hSAP ($n = 6$ per group). (**F**) Graph showing effect of different doses and frequencies of hSAP on Trichrome-stained fibrosis. qd, every day. (**G**) Immunofluorescence of αSMA-positive (a myofibroblast marker) area in kidneys of *Coll-*

*GFP* mice on d7 after UUO treated with HSA or hSAP (left panel), and percent of αSMA-positive cells that were Coll1a1-GFP–positive in kidneys treated with SAP or HSA (right panel). Note: hSAP inhibits Coll1a1 gene transcription in kidney myofibroblasts. Marker, 50 μm. (**H**) Morphometric quantification of F4/80 positive (a macrophage marker) area on d7 after UUO in kidneys of mice treated with HSA or hSAP ($n = 6$ per group). *$P < 0.05$, **$P < 0.01$.

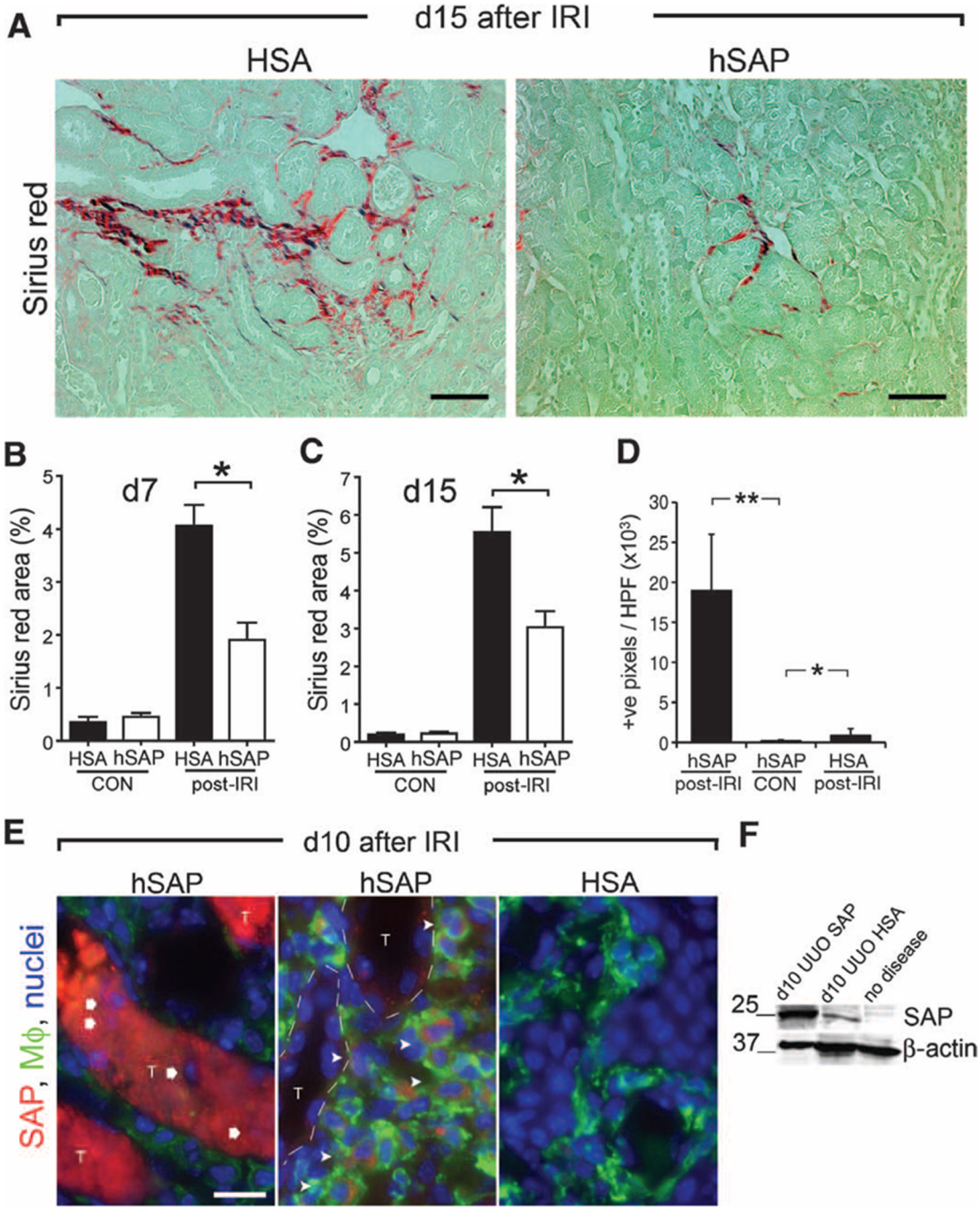


**Fig. 2.**

SAP inhibits fibrosis after IRI and is selectively deposited in the injured kidney. (**A**) Sirius red stain of d15 post-IRI kidneys in C57BL6 mice treated with HSA or hSAP (20 mg/kg q2d) (marker, 100 μm). (**B** and **C**) Morphometric quantification of Sirius red area in (B) d7 post-IRI kidneys or (C) d15 post-IRI of mice treated with HSA or hSAP. (**D**) Morphometric quantification of SAP deposition detected by immunofluorescence in d7 post-IRI kidney treated with hSAP or HSA compared with a control, nondiseased kidney. (**E**) Immunofluorescence images (left panel) of SAP (green) detected in post-IRI kidney after alternate-day intraperitoneal injections of hSAP or HSA. Note that SAP is detected in intratubular cellular debris (left) where nuclear debris can be seen (arrows), but is also seen in

interstitial macrophages (F4/80, green) (center) predominantly in endosomes and phagosomes (arrowheads) (**F**) Western blot of whole-kidney proteins detecting SAP in kidneys d10 after UUO and normal kidney. $n = 6$ per group. Marker, 50 μm. $^{*}P < 0.05$, $^{**}P < 0.01$.

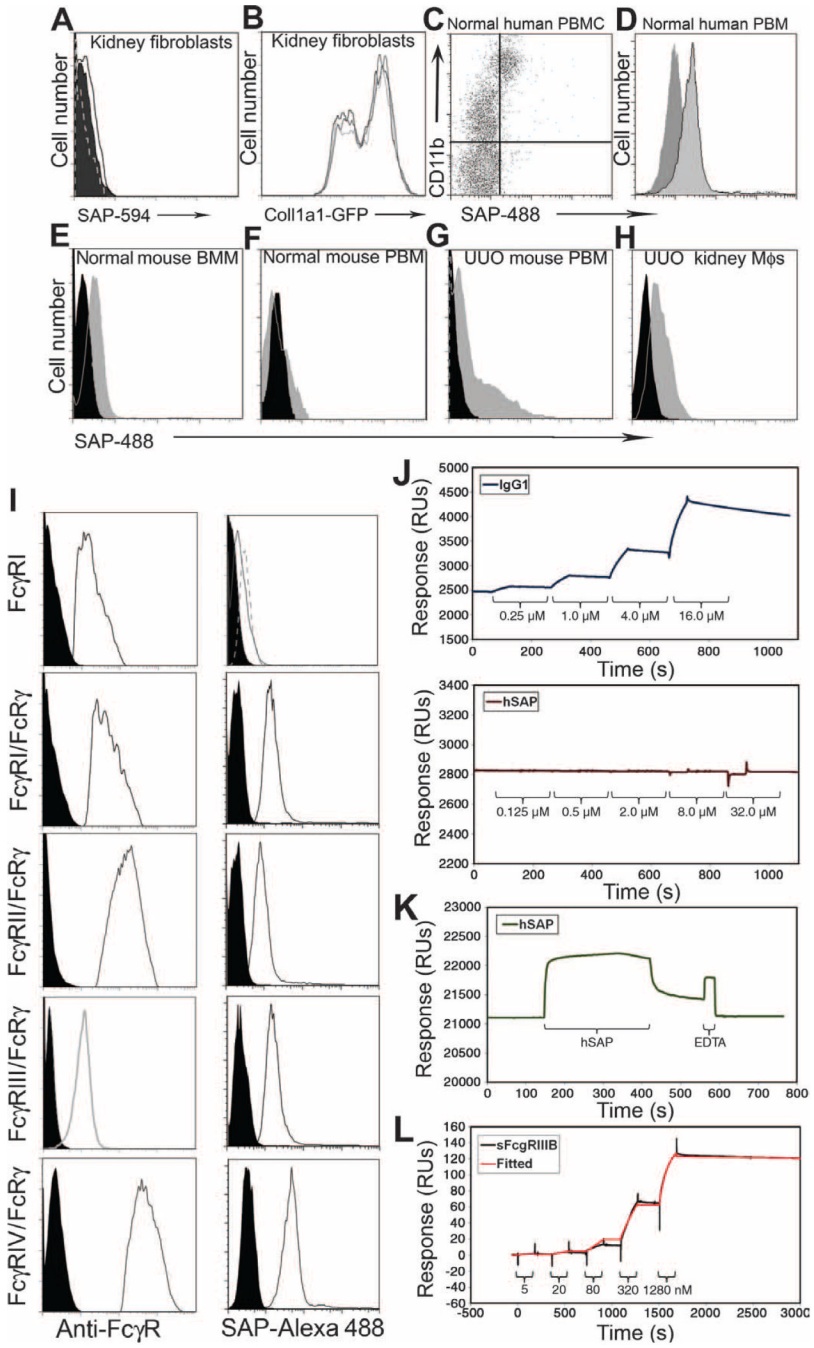


**Fig. 3.**

SAP binds to the surface of monocyte lineage cells and FcγRs. (**A**) Histogram plot of binding of SAP-594 compared with that of HSA-594 to primary cultured mouse kidney interstitial fibroblasts purified from *Coll-GFP* mice. (**B**) Histogram plot of *Coll-GFP* fluorescence intensity in primary kidney fibroblasts from *Coll-GFP* mice cultured for 24 hours with HSA (50 μg/ml; black), hSAP (25 μg/ml; gray), or hSAP (50 μg/ml; light gray). (**C**) Plot of SAP-488 binding to human PBMCs separated by CD11b. SAP-488 binds selectively to CD11b high leukocytes (monocytes) (high FSC, low SSC) and does not bind to other leukocytes. (**D**) Histogram showing binding of HSA-488 (dark gray) and SAP-488 (light gray) to human monocytes. (**E** to **H**) Histograms showing HSA-488 (black) or SAP-488 (white) binding to (E)

purified, mature mouse BMMs, (F) mouse PBM from healthy mice, (G) PBM from mice d7 after UUO, (H) purified kidney macrophages from mice d7 after UUO compared. (**I**) Histogram plots of 3T3 mouse fibroblast cell lines expressing individual FcγRs with or without the co-receptor FcRγ-chain. Cell surface FcγR expression (white) is shown for individual cell lines (left columns) compared with isotype control (black). Binding of SAP-488 (white) compared with HSA-488 (black) is shown for individual cells lines (right columns). 7-AAD-positive cells are excluded from these binding studies. (**J** to **L**) Biochemical characterization of hSAP binding to hFcγRs with Biacore surface plasmon resonance technology. (J) Sensorgrams of human $IgG_1$ (upper panel) binding to hFcγRI (recombinant ectodomain) when the receptor is immobilized on a Biacore CM5 dextran chip, but hSAP (lower panel) was unable to bind to hFcγRI in this orientation. (K) Sensorgram of $Ca^{2+}$-dependent binding of hSAP to CM5 dextran followed by dissociation in the presence of $Ca^{2+}$ chelation (10 mM EDTA). (L) Sensorgram of single-cycle kinetic analysis of hFcγRIIIB binding to chip-bound hSAP oriented through $Ca^{2+}$-dependent binding to the CM5 dextran. Five different receptor concentrations injected in order of increasing concentration were used to obtain data for affinity calculation. Association time was 180 s and the final long dissociation was 7200 s for hFcγRIIIB (attenuated for presentation). Both raw data (black) and data fitted for 1:1 binding (red) are shown on the same sensorgram and represent data after background subtraction. Off-rate is very slow and drives the high affinity of interaction we observed. Results are representative of three independent experiments for each FcγR.

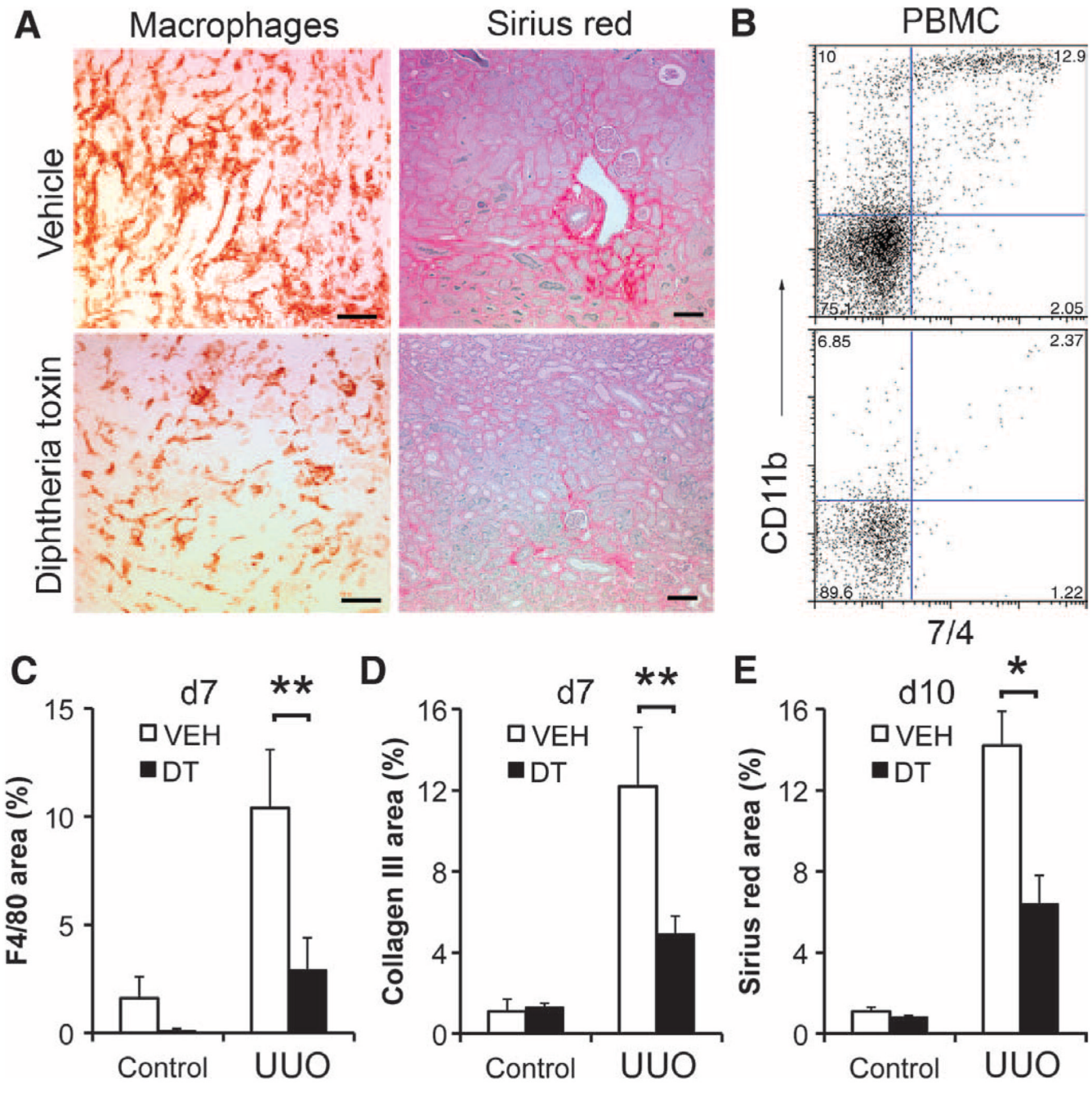


**Fig. 4.**

Conditional macrophage ablation inhibits kidney fibrosis in ureteral obstruction. (**A**) Photomicrographs of F4/80 immunostaining for macrophages or Sirius red staining for fibrosis in *CD11b-DTR* kidneys treated with DT or vehicle to ablate macrophages on d10 after UUO. (**B**) FACS plots of PBMCs from the same mice labeled with antibodies against CD11b and 7/4 to label monocytes, showing that DT also ablated circulating monocytes. (**C** to **E**) Morphometric quantification of F4/80 immunostain (C), collagen III immunostain (D) or Sirius red stain in kidneys 10 days after UUO in vehicle (VEH)-treated or DT-treated *CD11b-DTR* mice. **P* < 0.05, ***P* < 0.01.

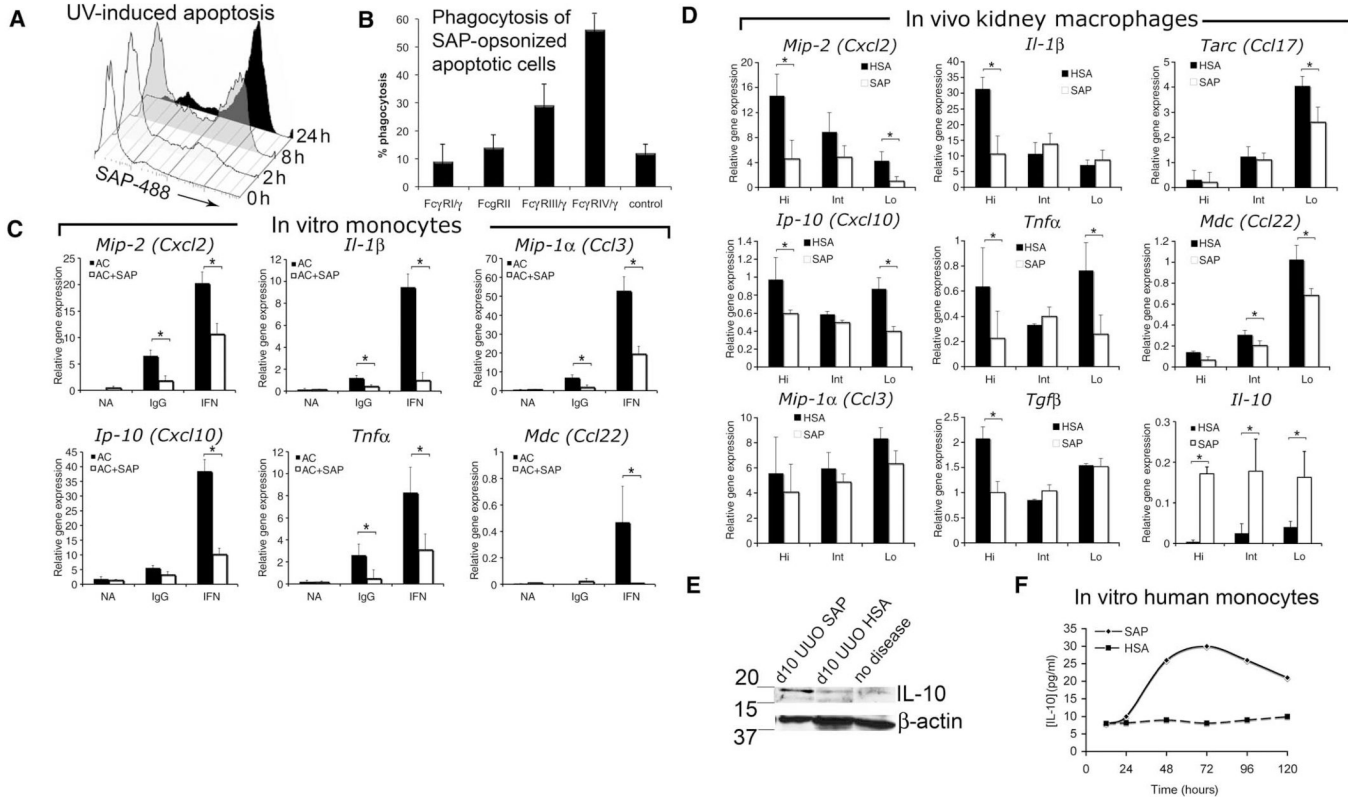


**Fig. 5.**

hSAP inhibits activation of mouse monocytes and kidney macrophages in vivo and ex vivo by triggering FcγR-dependent uptake of hSAP-opsonized apoptotic cells. (**A**) Histogram plots showing a time course (hours) of SAP-488 binding to Jurkat T lymphocytes after UV irradiation to induce apoptosis. (**B**) Representative plot of percentage phagocytosis of hSAP-opsonized apoptotic thymocytes by 3T3-FcγR/FcRγ-chain cell lines after a 4-hour co-incubation. (**C**) Relative transcript expression, assessed by bDNA amplification (normalized to housekeeping gene *Hprt1*), by purified mouse BMMs incubated with apoptotic cells (AC), unopsonized (black) or opsonized with hSAP (white), and coactivated with either no stimulus, immobilized IgG, or IFN-γ. (**D**) Relative transcript expression, assessed by bDNA amplification (normalized to housekeeping gene HPRT1) by three subpopulations of purified kidney macrophages 7 days after UUO, distinguished by the markers Ly6C$^{hi}$, Ly6C$^{int}$, and Ly6C$^{lo}$, from mice treated with HSA (black) or hSAP (white) by intraperitoneal injections for 7 days. In addition, relative *Il-10* transcript expression assessed by Q-PCR (normalized to housekeeping gene GAPDH) is markedly increased in all kidney macrophage populations by hSAP treatment. (**E**) Western blot of whole-kidney lysates showing IL-10 (18 kD) in d10 UUO kidneys of mice treated with hSAP but only weakly detected in mice treated with HSA. (**F**) Human monocytes incubated with SAP (5 μg/ml) triggers release of IL-10 protein in supernatants ($n = \geq 3$ per group, $^*P < 0.05$).

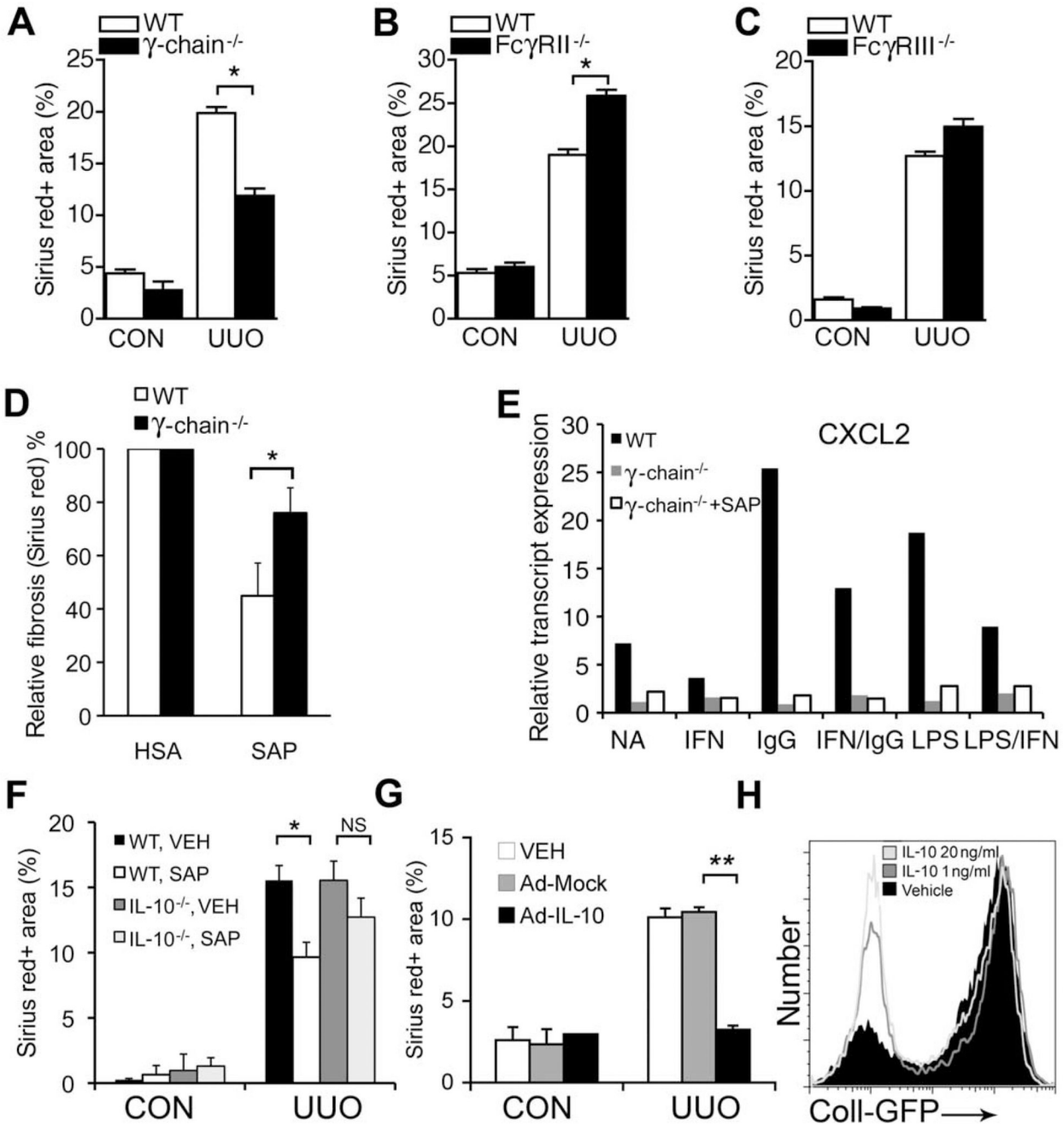


**Fig. 6.**

hSAP-inhibited kidney fibrosis is dependent on FcγR and IL-10 expression. (**A** to **C**) Morphometric quantification of Sirius red–stained kidney fibrosis 10 days after UUO in age- and strain-matched wild-type (WT) mice compared with (A) FcRγ-chain$^{-/-}$ mice (lacking FcγRI, III, and IV), (B) FcγRII$^{-/-}$ mice, and (C) FcγRIII$^{-/-}$ mice. (**D**) Morphometric quantification of Sirius red fibrosis. hSAP treatment of FcRγ-chain$^{-/-}$ mice fibrosis results in a significantly smaller reduction in fibrosis on d10 after UUO compared with strain-matched wild-type mice treated with hSAP. (**E**) CXCL2 relative gene transcription 24 hours after activation with inflammatory cytokines (IFN-γ, iIgG, LPS, or combinations) by wild-type monocytes, FcRγ-chain$^{-/-}$ monocytes or FcRγ-chain$^{-/-}$ monocyte coactivated with hSAP (25

μg/ml). (**F**) Morphometric quantification of Sirius red–stained kidney fibrosis d10 after UUO in strain-matched wild-type and IL-$10^{-/-}$ mice, treated with either HSA or hSAP. (**G**) Morphometric quantification of Sirius red–stained kidney fibrosis 10 days after UUO in C57BL6 mice treated systemically with Ad-IL-10, Ad-Mock, or no virus. (**H**) Histogram plots of cultured *Coll-GFP* kidney fibroblasts incubated with IL-10 for 8 hours assessed by flow cytometry show decreased *Coll1a1* gene transcription. ($n = 6$ per group; $^{*}P < 0.05$, $^{**}P < 0.01$).

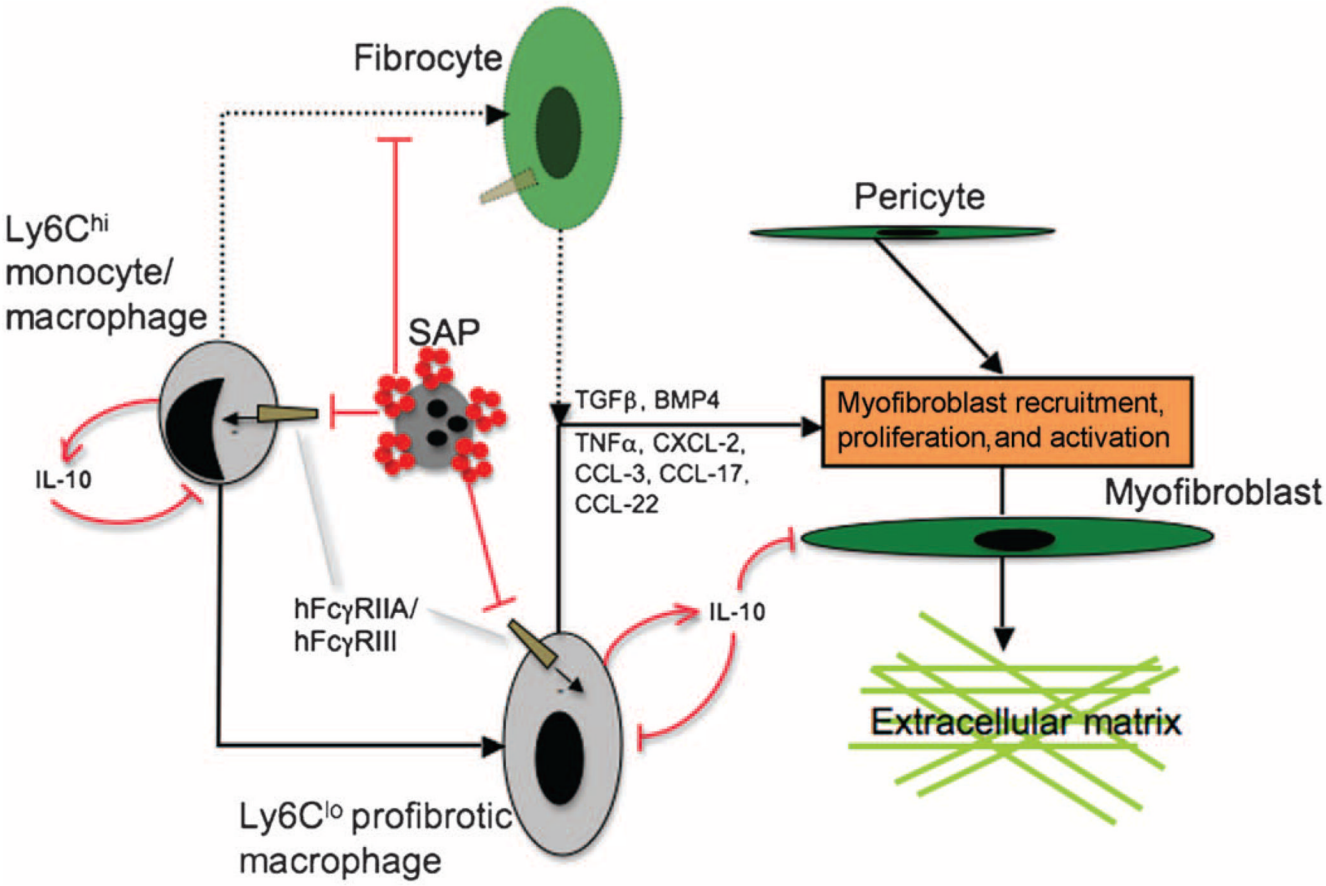


**Fig. 7.**

The antifibrotic mechanism of action of SAP. Apoptotic cells or debris are opsonized by SAP, which in turn renders SAP a high-affinity ligand for hFcγRIIA or hFcγRIII. Both Ly6C$^{hi}$ and Ly6C$^{lo}$ inflammatory macrophages bind SAP-opsonized debris, which triggers IL-10 release, inhibiting macrophage profibrotic function (through recruitment and activation of pericytes/ myofibroblasts) and directly inhibiting myofibroblast production of collagen 1a1. Although SAP inhibits fibrocyte appearance, fibrocytes play no role in kidney fibrosis.

## Table 1

Affinities of FcγRs for human SAP. Single-cycle kinetics methods and analysis on the Biacore X100 were used to obtain binding affinities for interaction of different hFcγRs with hSAP. The SAP was oriented via $Ca^{2+}$-dependent dextran binding to the chip. For each analysis, an ascending concentration series of five different hFcγR concentrations was used. The results shown represent the average of at least two separate analyses for each receptor.

| FcγR | $K_D$ (M) |
|---|---|
| hFcγRI | $4.3 \times 10^{-9}$ |
| hFcγRIIA (H131) | $2.9 \times 10^{-10}$ |
| hFcγRIIB | No binding |
| hFcγRIIIB | $3.7 \times 10^{-10}$ |